JACS
JOURNAL OF THE AMERICAN CHEMICAL SOCIETY
pubs.acs.org/JACS
Article

Hierarchical Self-Assembly of Nanowires on the Surface by Metallo-Supramolecular Truncated Cuboctahedra

Heng Wang,[#] Kun Wang,[#] Yaping Xu,[#] Wu Wang,[#] Shaohua Chen, Matthew Hart, Lukasz Wojtas, Li-Peng Zhou, Lin Gan, Xuzhou Yan, Yiming Li, Juhoon Lee, Xian-Sheng Ke, Xu-Qing Wang, Chang-Wei Zhang, Shasha Zhou, Tianyou Zhai, Hai-Bo Yang, Ming Wang, Jiaqing He, Qing-Fu Sun, Bingqian Xu, Yang Jiao, Peter J. Stang, Jonathan L. Sessler,* and Xiaopeng Li*

Cite This: *J. Am. Chem. Soc.* 2021, 143, 5826−5835

Read Online

ACCESS | Metrics & More | Article Recommendations | Supporting Information

ABSTRACT: Parastichy, the spiral arrangement of plant organs, is an example of the long-range apparent order seen in biological systems. These ordered arrangements provide scientists with both an aesthetic challenge and a mathematical inspiration. Synthetic efforts to replicate the regularity of parastichy may allow for molecular-scale control over particle arrangement processes. Here we report the packing of a supramolecular truncated cuboctahedron (TCO) into double-helical (DH) nanowires on a graphite surface with a non-natural parastichy pattern ascribed to the symmetry of the TCOs and interactions between TCOs. Such a study is expected to advance our understanding of the design inputs needed to create complex, but precisely controlled, hierarchical materials. It is also one of the few reported helical packing structures based on Platonic or Archimedean solids since the discovery of the Boerdijk−Coxeter helix. As such, it may provide experimental support for studies of packing theory at the molecular level.

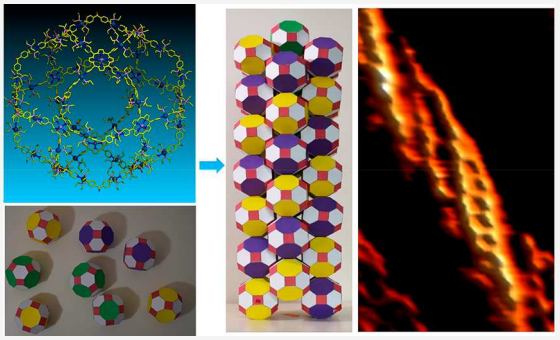

INTRODUCTION

Ordered systems with a high degree of regularity are ubiquitous in nature and include such canonical constructs as the double helix of DNA[1] and the protein sheath of the tobacco mosaic virus.[2] The underlying aesthetics have fascinated artists and inspired scientists for centuries. When observed from a particular viewpoint, a class of natural ordered arrangements, typically referred to as parastichy in botany, gives rise to helical patterns, as seen in the leaves, florets, and bracts of certain plants.[3] An understanding of parastichy has advanced our understanding of plant growth and has led to advances in mathematics that, in turn, have helped with the classification of plants.[2−5] For instance, the bracts on the surface of pineapples (shown in Figure 1a) are designated as (5, 8, 13) in the language of parastichy. These values represent three consecutive numbers within a Fibonacci sequence. The term parastichy has also been used to classify the tubular parts of bacteriophages as well as other natural existing or theoretical possible patterns on tubes.[2] More broadly, the study of natural and artificial systems containing an ordered arrangement of subunits, e.g., DNAs,[1] proteins,[6] supramolecular columns,[7−9] etc., has revealed intriguing connections between number theory and packing theory.[2,4,5] The resulting insights are inspiring current efforts to design and synthesize novel materials with desirable properties.[10] Nevertheless, generating systems with helical order, including those that mimic parastichy, remains a challenge. This is particularly true for particles packed at the nano- and molecular scale.[11]

Building on the principles of coordination-driven self-assembly,[12−29] we have now prepared a truncated cuboctahedron (TCO), one of the 13 Archimedean solids, which possesses six octagonal, eight hexagonal, and 12 square facets. On the surface of highly ordered pyrolytic graphite (HOPG), the present TCOs further assemble into nanowires. The resulting surface patterns are similar to those seen in botanic and biological parastichies with a double-helical (DH) pattern being readily apparent if viewed from a particular perspective (Figure 1b−d). This non-natural parastichy arrangement is classified as [4, 2](0, 1, 2) according to the nomenclature of parastichy theory.[2] This packing represents a subpacking of the 3D superstructure seen in a single-crystal X-ray diffraction-based solid-state structure. Thus, in contrast to botanic parastichies, which are governed by auxin and stress fields from shoot apical meristems,[3] the present system relies on relatively rigid subunits

Received: January 22, 2021
Published: April 13, 2021

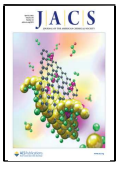

https://doi.org/10.1021/jacs.1c00625
J. Am. Chem. Soc. 2021, 143, 5826−5835

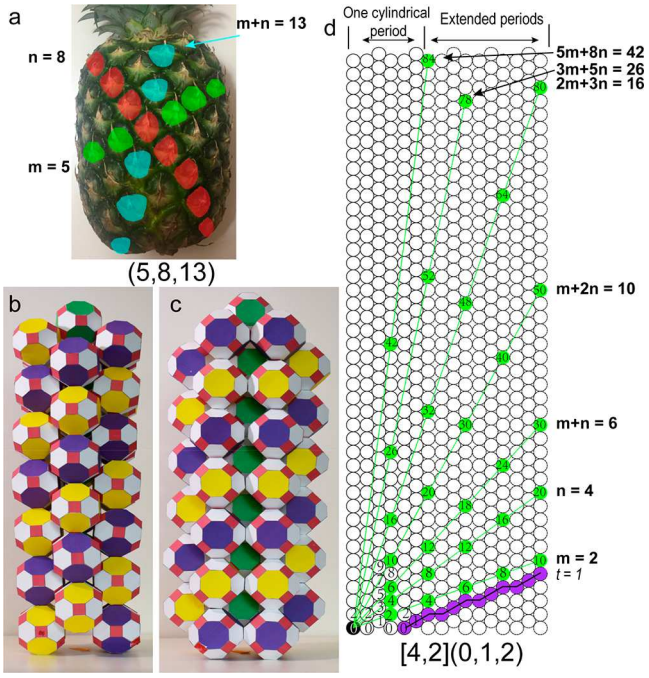

Figure 1. Natural and non-natural parastichy packings. (a) Pineapple showing the pattern-defining parastichy numbers (5, 8, 13). (b and c) Paper model of a TCO nanowire of this report highlighting the non-natural parastichy. (d) View of the cylindrical nanowire in b and c unrolled and flattened onto a plane along the long axis. The circles (TCOs) within a given level are assigned numbers used to categorize parastichies in plants per the Fibonacci sequence, e.g., 2, 4, 6, 10, 16, 26, and 42. A helical pattern with the non-natural t = 1 parastichy is highlighted in purple.

that support particle−particle and particle−substrate interactions in a controlled hierarchical fashion, as inferred from simulations. It also differs from the well-known Boerdijk−Coxeter helix, which is linearly packed with tetrahedra. Since the latter system was disclosed in 1952, very few new helical packing structures based on either the Platonic or Archimedean solids have been reported.[30−32] Were such arrangements available, they could provide new experimental predicates that would allow advances in packing theory to be made while increasing our understanding of the rules governing the self-assembly of complex functional materials. As a first step toward exploring this latter possibility, the nanowires formed from TCO on the HOPG surface were transferred to other substrates. This could be done without losing integrity. This has permitted further characterization studies and initial conductivity measurements as discussed further below.

RESULTS AND DISCUSSION

Self-Assembly and Characterization of the Complex.

As a prelude to our parastichy studies, we first assembled a discrete TCO using a 120° bent diplatinum(II) motif (DP) and a zinc 5,10,15,20-tetra(4-pyridinyl)-21*H*,23*H*-porphyrin (ZP) in a 2:1 ratio (Scheme 1). A ^{1}H NMR spectral analysis of the resulting TCO (Figure 2a) revealed characteristic downfield shifts for the pyridinyl protons. Such spectral shifts are consistent with the proposed coordination between the pyridinyl group and Pt(II). The broad nature of the signals may reflect slow tumbling motion on the NMR time scale as seen in other large symmetric structures.[20−22] A 2D diffusion-ordered NMR spectroscopy (DOSY) analysis in d_6-DMSO

Scheme 1. Self-Assembly of TCO from DP and ZP Ligands

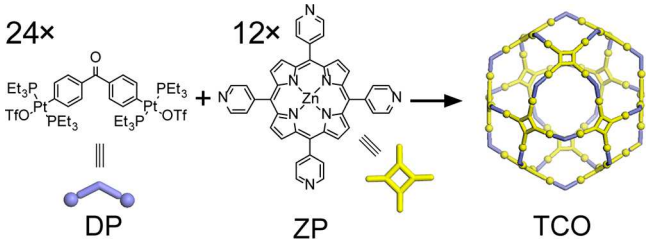

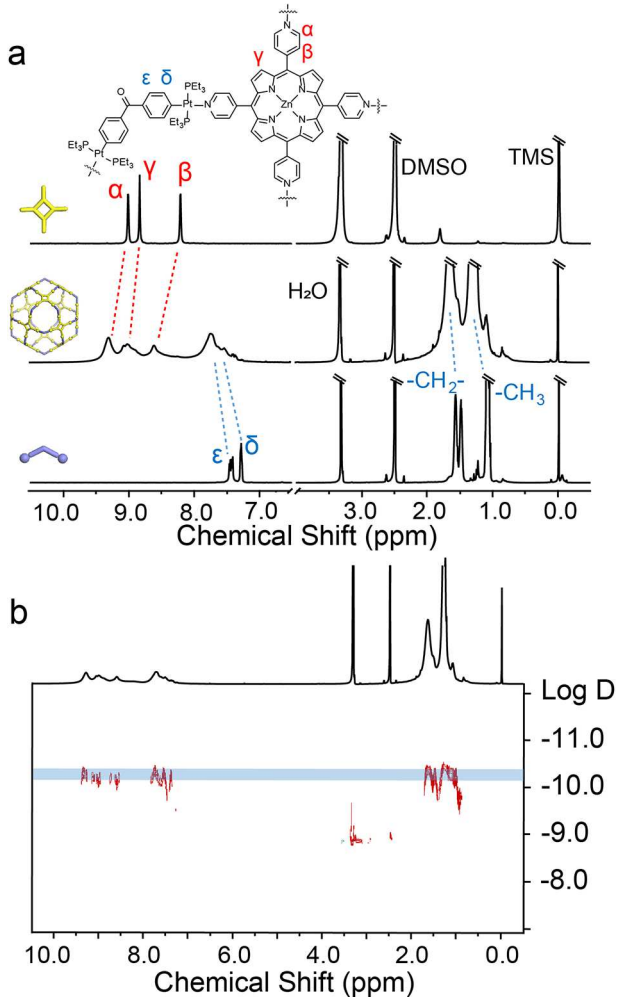

Figure 2. (a) ^{1}H NMR spectra (500 MHz, 298 K, solvent d_6-DMSO) of ZP (top), TCO (middle), and DP (bottom); (b) 2D DOSY spectrum of TCO.

revealed a single band at logD = −10.4 (Figure 2b), corresponding to a discrete architecture. The results of detailed NMR spectroscopic studies are summarized in the SI (Figures S5−S14).

After deconvolution of the ESI-MS spectrum (Figure 3a), the average molecular weight was determined to be 40328 + 78n Da, matching well with the formula of TCO ($[Pt_{48}(C_{37}H_{68}OP_4)_{24}(C_{40}H_{24}N_8Zn)_{12}]^{48+}\cdot 48(OTf^-)\cdot n(DMSO)$, n = 1−8, solvent adducts, Figure S15). Due to the limitation of our TOF analyzer, we were unable to obtain a fully satisfactory isotope pattern. However, an ion mobility−mass spectrometry (IM-MS) spectrum (Figure 3b) proved consistent with the formation of discrete and shape-persistent supramolecules free of other

https://doi.org/10.1021/jacs.1c00625
J. Am. Chem. Soc. 2021, 143, 5826−5835

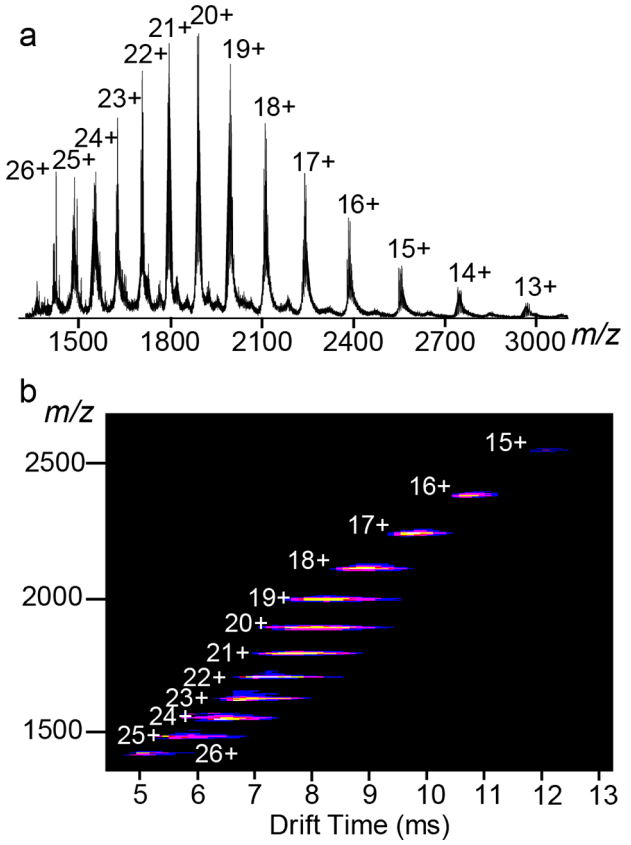

Figure 3. (a) ESI-MS and (b) TWIM-MS plots (m/z vs drift time) of TCO.

isomers. The results of atomic force microscopic studies (uniform dots, average height: ~5.6 nm, Figure S17) and transmission electron microscopy (average diameter: ~6 nm, Figure S18) provided further support for the proposed structure.

Single crystals (~ 50 μm, Figure S16) were obtained by slow diffusion of toluene vapor into a DMF solution of the presumed TCO. Synchrotron X-ray radiation was used to collect diffraction data. The size of the TCO led to a large unit cell (a = b = 68.6 Å; c = 77.3 Å; space group $I4/m$), as well as large structural voids encapsulating disordered contents. Thus, as true for several recently reported giant spherical supramolecules,[20−22,25,33] the TCO crystals might best be classified as clathrates instead of conventional single crystals. These limitations, coupled with the fragility of the crystals, resulted in diffraction data with a best resolution of 1.7 Å. This resolution is comparable to that of some protein crystallographic studies,[34] but is considerably lower than what is seen for typical small-molecule analyses.

In order to analyze the diffraction data, the crystallographic methods of protein and small-molecule crystallography were combined; this allowed us to build a model and refine the structure (for details see the SI). Although inadequate in terms of defining specific structural details, this crystallographic analysis did serve to confirm the connectivity/topology of the system as a whole and to establish the basic packing properties of the individual subunits. For instance, the electron density map allows us to conclude that 24 DPs and 12 ZPs are linked together to form a TCO with 12 solid squares, as well as eight hexagonal and six hollow octagonal faces, respectively (Figure 4 and Movie S1). The C_{4h} symmetry of the cage departs from an ideal O_h symmetry and presumably reflects distortions arising from the somewhat flexible nature of the subunits that make up the present TCO. It is important to appreciate that this particular TCO is among the largest metallo-supramolecular cages ever reported[20−22,25] and that the structural resolution is as good or better than that recorded for other superlarge metallo-ensembles. Nevertheless, the structural model derived from the X-ray diffraction data should be considered as supportive, rather than definitive, as would normally be the case for a small-molecular single-crystal-based diffraction analysis.

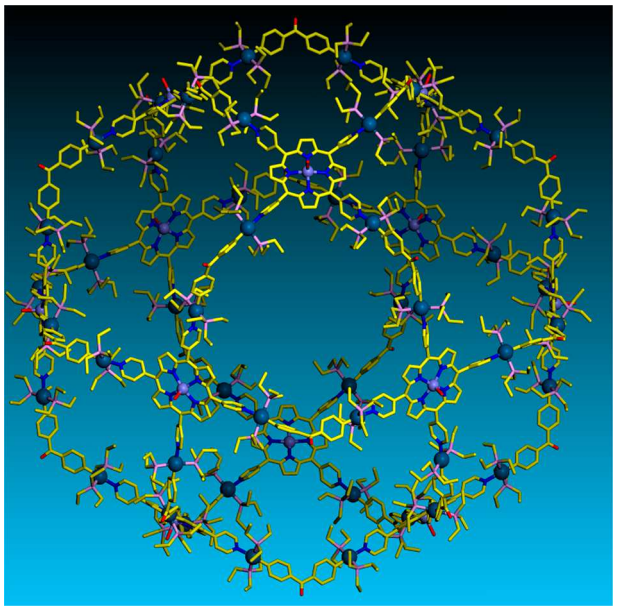

Figure 4. Crystal structure of a TCO.

Within the crystals, a body-centered-tetragonal (BCT) packing of distorted TCOs is observed. The ZP squares within one TCO are found to lie parallel and face-to-face with ZP squares present in adjacent TCOs, albeit with a slight lateral displacement. Solvent (dimethylformamide, DMF) and counterions (triflate anions) are present between the porphyrin planes. The interplanar distances between ZPs depend on the specifics of these intervening species, being 7.08 Å when only DMF is present between the planes and 10.5 Å when both DMF and counterions are present between the planes (Figure S1). The cofacial orientation of the porphyrins in the TCOs is thus reminiscent of the bacteriochlorophyll dimer seen in the special pair of photosynthetic bacteria.[35] However, the nature of the stabilization differs. Rather than $\pi-\pi$ donor−acceptor and protein-based effects, in the case of the packed TCOs, it is porphyrin-solvent/counterion-porphyrin arrangements that serve to bring the adjoining porphyrins into close proximity. Presumably, the presence of counteranions and solvent molecules serves to reduce the electron repulsion that would otherwise arise as the result of the Pt(II) ions surrounding each ZP. The net result is a diffuse porphyrin−porphyrin contact (termed Por−Por) between individual TCO "building blocks".

Packing of TCOs on a HOPG Surface. Given their ability to interact through Por−Por contacts, we set out to explore the packing behavior of the TCOs on HOPG. We appreciated that porphyrins are able to form ordered arrays on either liquid/solid or air/solid interfaces.[36−41] We thus expected to obtain a 2D monolayer of TCOs on HOPG as the result of putative stabilizing $\pi-\pi$ interactions between the ZP squares and the graphite surface.[40−42] However, to our surprise drop-casting a TCO solution in DMF on HOPG and allowing for only a short

https://doi.org/10.1021/jacs.1c00625
J. Am. Chem. Soc. 2021, 143, 5826−5835

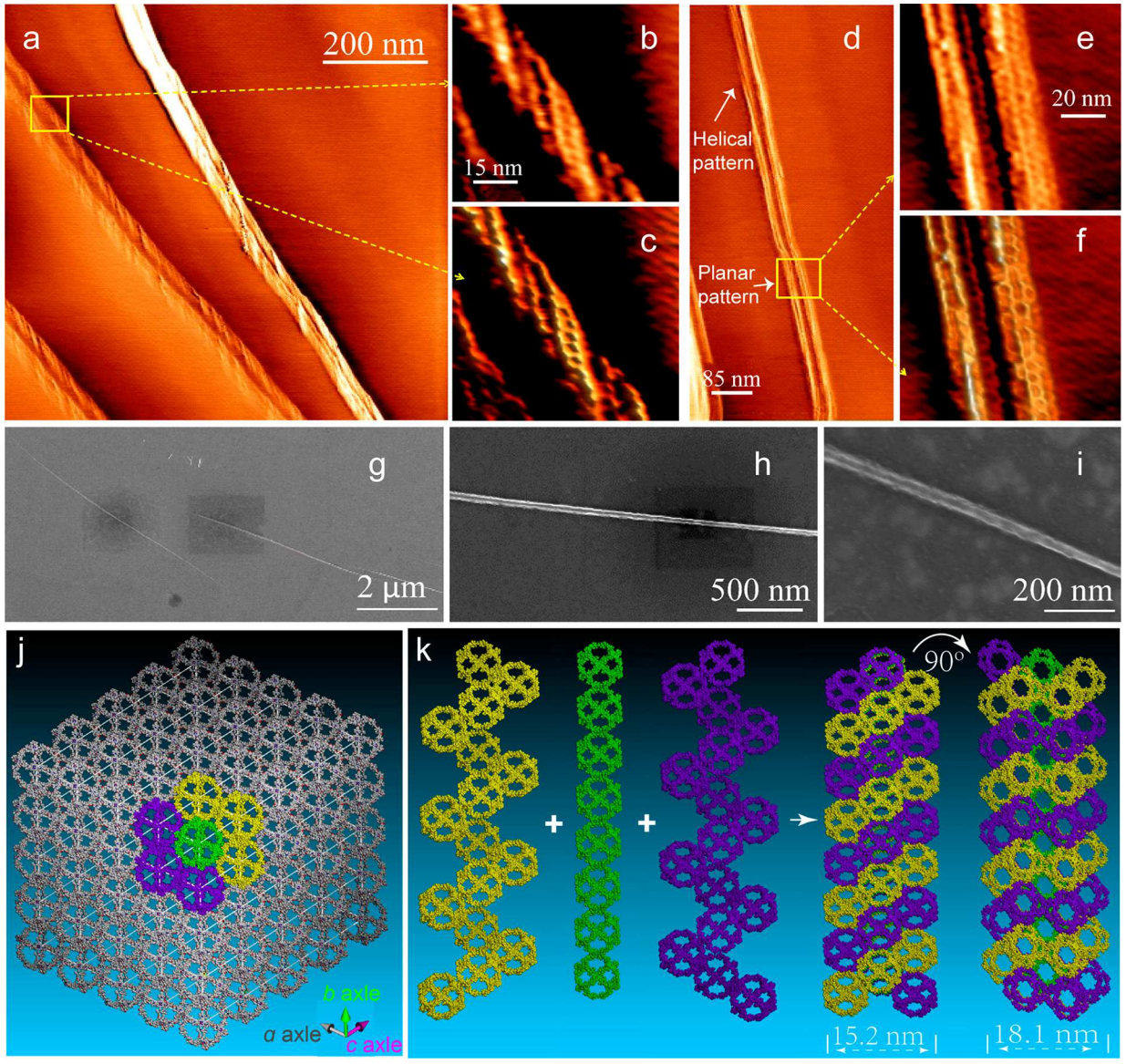

Figure 5. (a) STM imaging of twin nanowires. Zoomed-in images of the nanowires grown on (b, c) the step edges and (d–f) the basal plane of HOPG. (g–i) SEM imaging of ultralong nanowires on HOPG. DH pattern extracted from the crystal lattice: (j) top view and (k) side view, helical pattern composed of double helically and linearly arranged TCOs; planar pattern viewed by rotating the helical pattern by 90°.

incubation time (<30 s) gave rise to DH nanowires with ultralong lengths and uniform diameters, as inferred from scanning tunneling microscopy (STM), scanning electron microscopy (SEM), and atomic force microscopy (AFM) (Figure 5a–i, Figures S19–S21) studies carried out under ambient conditions. Elemental mapping images (Figure 6b–f) and an energy-dispersive X-ray spectrum (EDX) (Figure S19) of the nanowires revealed the presence of all the elements making up the TCO building blocks. Control STM studies involving, for example, clean or solvent-treated HOPG were carried out; none of these controls gave rise to the DH nanowire patterns (Figure S24). We further conducted 1D small-angle X-ray scattering results (SAXS) to characterize the 1D nanowires that we propose form on the HOPG (for details see the SI). The SAXS curve (Figure S26, 48 h incubation time) shows peaks at $q \approx 0.9$ and 0.6 $Å^{-1}$ with spacing of ca. 0.7 and 1.1 nm, respectively. These distances correspond to what would be expected for the two types of TCO–TCO spacings inferred from the single-crystal data (Figure S1).

Zoomed-in STM images revealed more detailed packing information for the TCOs present on the substrate (Figure 5b–f). Specifically, two types of patterns are observed, i.e., helical patterns with a relatively narrow diameter (~15 nm, right-handed shown in Figure 5b,c, left-handed shown in Figure S20) and planar (Figure 5d–f) patterns with broader diameters (~20 nm). The helical patterns are mainly found on the step edges of HOPG, whereas the more planar ones are mostly observed on the HOPG basal planes. Based on precedent provided by other self-assembly studies, we suggest that all the observed nanowires actually assemble on the step edges due to step edge decoration.[43] Although further analysis is needed, we propose that the twist or handedness of the helical pattern is induced by the helical structures of the step edge.[44] To the extent such thinking is correct, the planar patterns observed on the basal plane would have their origin on the step edges and then be displaced/rotated during sample preparation.

Notably, helical patterns were observed together with planar patterns. These deformations are ascribed to the extremely large

https://doi.org/10.1021/jacs.1c00625
J. Am. Chem. Soc. 2021, 143, 5826–5835

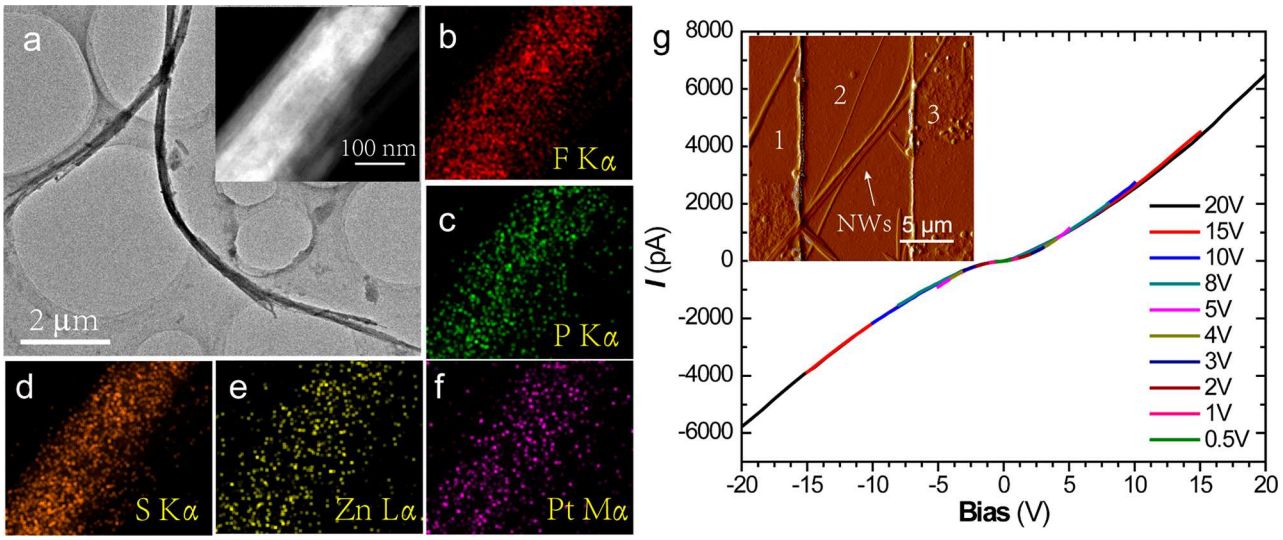

Figure 6. (a) TEM image of bundles of transferred nanowires on a lacey carbon supported Cu grid; (right inset) zoomed-in HAADF-STEM (high-angle annular dark-field scanning transmission electron microscopy) image used for element mapping. (b–f) Element mapping of selected areas. (g) *I*–*V* characteristics at a series of different bias voltages for the transferred nanowires (marked as NWs) between contacts 1 and 3 (left inset).

length-to-diameter ratio of the DH nanowires (10^4). This leads to insufficient stiffness to maintain rotational integrity and prevent twisting (helical pattern reason). In the event, all of the nanowires observed on the step edges of the HOPG were found to occur as closely spaced parallel pairs. These unique packing characteristics are ascribed to the so-called Smoluchowski effect[45] as well as to the adsorbate-induced surface electronic perturbations that are often seen when small organic molecules pack onto metal surfaces[46,47] (cf. the SI for a more detailed discussion).

Based on the dimensional information inferred from the STM studies, a paper model for the DH nanowire was constructed, along with animation models leading to its formation. These studies provide support for a structure wherein all the TCOs are packed such that the individual squares are oriented in a face-to-face manner stabilized via putative interparticle interactions involving the ZPs (Figures 1b,c and S41; Movies S2 and S3). The contact between the helical patterns shown in Figure 1b,c and the arrangement of the ZP squares on the HOPG are ascribed to stabilizing interactions involving the ZP subunits. These interactions can include direct π–π donor–acceptor contacts or the anion and solvent bridging charge neutralization effects discussed above. The net result is that in all cases the ZP subunits can self-assemble further via Por–Por interactions.

We reasoned that the arrangement of the individual TCOs within the nanowires on the HOPG surface should reflect interactions that are consistent with what is seen in the 3D packing observed within the single crystal subject to X-ray diffraction analysis. On the basis of this assumption, we extracted a DH nanowire pattern from the crystal structure along the body diagonal axis of the unit cell with a hexagonal cross section containing seven polyhedra (Figures 5j and S2). This particular nanowire is formed by wrapping two helices (yellow and purple) around a straight rod (green) using the same dimensions derived from the STM imaging. Each TCO within the central rod is surrounded by 12 TCOs via interactions involving ZP squares. Helical and planar patterns can also be seen when the extracted superstructure is rotated along its long axis (Figure 5k, Movie S4).

Using the methods developed to characterize parastichy,[2] we analyzed the non-natural helical arrangement of TCOs on the wall of the nanowire without considering the central rod. To do this, each TCO was represented by a circle. An unrolled plane was then obtained by cutting the nanowire along its long axis (Figure 1d, Movie S5). This analysis revealed a parastichy number, $t = 1$, that is exceptionally rare in nature. The DHs propagate as a zigzag spiral stair and are formally named as [4,2](0,1,2). Detailed descriptions of the naming schemes for parastichies are provided in the SI.

Transferring the DH Nanowires off HOPG for Fabricating Devices. To investigate the physical properties of the self-assembled nanowires for potential applications in nanoelectronic devices, we transferred the ensembles formed on HOPG onto other substrates (for details see SI, Figure S33). AFM (Figures S27, S34, S35), transmission electron microscopy (TEM, Figure 6a and Figures S28–S31), and elemental mapping images (Figure 6b–f) were then recorded. Notably, the characteristic elements of the TCO framework, as well as those of the counterions (i.e., P, Zn, Pt, F, and S; and Figure S32, Table S2), were observed. This was taken as support for the suggestion that the integrity of the nanowires remained intact after transfer. The nanowires are likely to bundle together during the transfer process (Figures S28 and S29). In the case of the nanowires transferred onto an ultrathin carbon-coated Cu grid, separated twin nanowires could be observed as closely spaced parallel pairs at the edge regions of the bundled wires. High-resolution TEM (HRTEM) images were collected on a set of twin nanowires. The electron beam dose was carefully controlled to prevent damaging the nanostructure (see SI for details, Figure S30). Lamellar patterns were clearly observed with a *d*-spacing around 0.75 nm (Figure S31), which agrees well with the image based on the DH nanowire model with Zn and Pt atoms only (Figure S31j), as well as the SAXS data recorded for nanowires on HOPG surfaces (Figure S26). Although ostensibly different patterns were observed via HRTEM and STM, it is important to appreciate that HRTEM reflects the nanostructures, while STM probes the surface morphology.

After transferring the nanowires onto a SiO_2/Si substrate with Au/Cr contacts, we carefully recorded the *I*–*V* curve of the

https://doi.org/10.1021/jacs.1c00625
J. Am. Chem. Soc. 2021, 143, 5826–5835

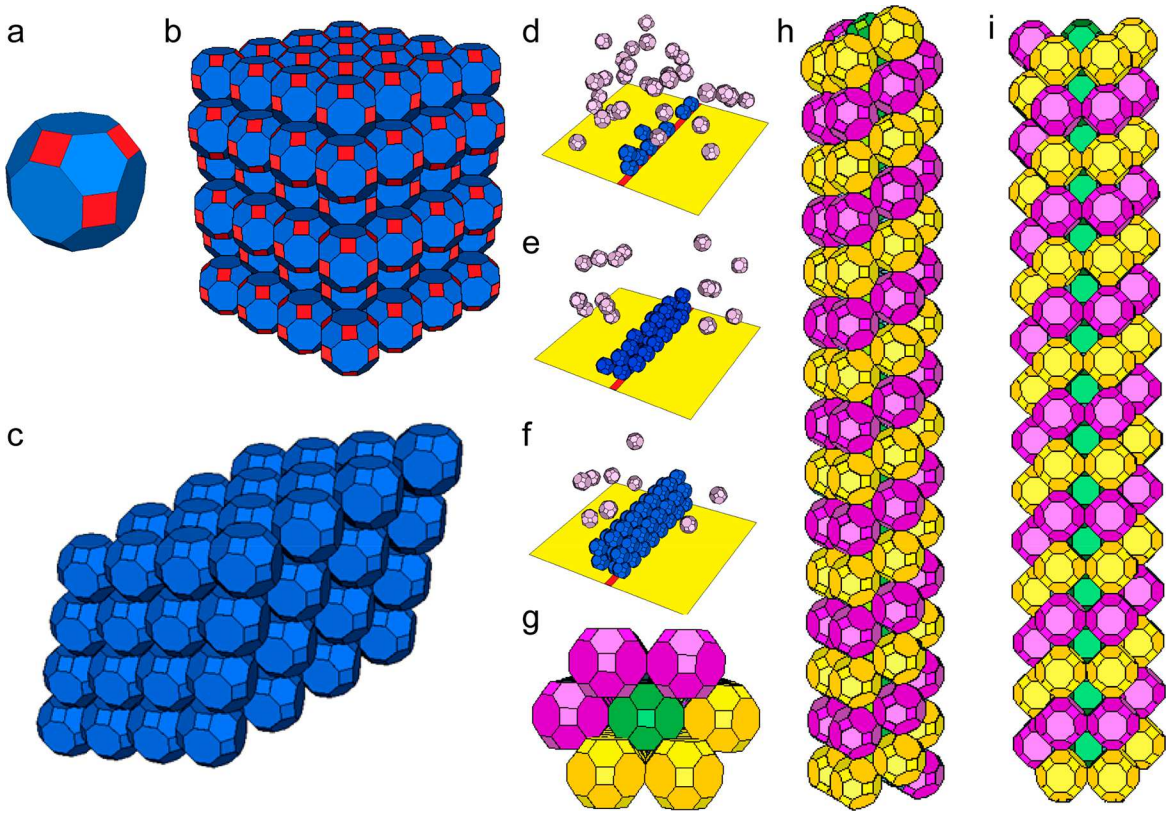

Figure 7. Simulation of the TCO packing leading to DHs. (a) TCO model with porphyrin-based faces (in red) capable of interacting with other such domains. (b) Portion of the hierarchical structure resulting from the simulated packing of TCOs with Por−Por interactions (see text for definition) whose self-assembly process is enthalpy-dominant. (c) Assembly of TCOs without considering Por−Por interactions under an entropy-driven scenario. (d−f) Simulated self-assembly process of the DH packing of TCOs including Por−Por interactions along the step edge on an HOPG surface. (g) Top and (h, i) side views of the 1D packing of the TCOs with Por−Por interactions in the DHs; this model proved consistent with the experimentally obtained 1D superstructure.

resultant device by applying various bias voltages (Figures 6g and S36 and S37). Characteristic conductivity $I-V$ curves with highly symmetric shapes were obtained at all applied voltages (0.5−20 V; average resistance: 8.0 ± 2.7 GΩ), with high stability and reproducibility (Figures S36 and S37). $I_{DS}-V_{GS}$ curves of the transferred devices were tested, and the results are shown in Figure S39. From the curve we could calculate the on−off ratio as 3.2, the mobility as being ca. 9×10^{-2} $cm^2 \cdot v^{-1} \cdot s^{-1}$, and that the device acts as a p-type semiconductor. Since the distance between every two cages is beyond the $\pi-\pi$ interaction range for electronic conduction, the conductivity of the devices could come from contacts between the porphyrin-Pt(II) subunits (with 8+ charges around each porphyrinic unit) as a result of thermal motion, which leads to p-type mobility. The fact that these transferred nanowires display high stability and good reproducibility leads us to speculate that they could find potential applications for fabricating p-type nanoelectronic devices. We thank a reviewer of this article for calling this possibility to our attention.

Simulations of the Packing. To understand better the DH pattern using packing theory, the TCOs were modeled as perfect hard polyhedral particles, with and without considering Por−Por interaction. This was done so as to mimic the effects of the porphyrin-solvent/counterion (DMF/triflate)-porphyrin interactions seen in the solid state (*vide supra*), as well to explore what might be expected in their absence (Figure 7). Adaptive-shrinking-cell Monte Carlo (MC) simulations were then performed using these two limiting hard particle models.[48] Recent studies have indicated that the self-assembled superstructures are intimately related to the dense ordered packings of the constituent building blocks in 3D Euclidean space.[48−51] The corresponding self-assembly process can be either driven by directional entropic forces to maximize the face−face contacts between the particles[50] or driven by facet−facet interactions between the building blocks.[52,53] In the present instance, the individual components are monodispersed TCOs with distinct, porphyrin-based interacting faces; this stands in contrast to most previous experimental studies that relied on the use of polydispersed nanoparticles as the building blocks.[54−57]

We first analyzed hard TCOs without considering the proposed Por−Por interactions. Under this scenario, the TCOs were found to self-assemble into a Bravais lattice packing with a triclinic unit cell and a packing fraction (amount of space covered by the particles) $\varphi \approx 0.849$ (Figure 7c). Such a relatively dense packing is consistent with the reported theoretical[48] and experimental (involving metallic nanoparticle systems)[54] packing arrangements seen for centrally symmetric polyhedral particles driven by entropy. Next, we introduced Por−Por interactions on the square facets as done in the case of other models.[53] This allows for an effective finite-ranged attraction between a pair of square facets, the details of which depend on the projected overlapping area, the center-to-center distance, and the dihedral angle between the two facets (see SI for details). As shown in Figure 7a,b, with this model the TCO particles self-assemble into face-centered-cubic (FCC) arrangements with a packing fraction $\varphi \approx 0.688$ wherein each particle

https://doi.org/10.1021/jacs.1c00625
J. Am. Chem. Soc. 2021, 143, 5826−5835

contacts 12 neighbors through Por−Por interactions. Although free of the slight distortions seen in the X-ray crystal structure discussed above, the simulated FCC packing is fully consistent with the experimental results. This leads us to conclude that self-assembly processes involving the TCOs will be dominated by facet Por−Por interactions.

Finally, efforts were made to simulate the self-assembly leading to the formation of the observed single nanowire along the step edge of HOPG under conditions of short incubation times. In contrast to what is true for the packing of polyhedra in 3D infinite space and other confined geometries,[29,54−58] little is known about the determinants governing assembly in such more-open surface environments. The geometrical constraints provided by the HOPG step edge were modeled by employing hard-wall conditions at the bottom (and top) boundary of the simulation domain. Periodic boundary conditions were used for the other boundaries. In addition, we introduced a straight belt on the bottom wall of the simulation domain to model the substrate−ZP interactions and the attraction between square facets of individual TCOs at the step edge due to the Smoluchowski effect[45] (see SI for details). With the temperature kept at T_0 during the simulation, the initial packing fraction was found to be $\varphi \approx 1\%$, a value that increased slowly as the distance between the bottom and top wall was reduced. During the initial stages of the simulation, a column of TCOs nucleates and deposits on the belt (step edge), with the square facets attaching to the surface as the result of the "sticky" interactions between the ZP squares and the graphite surface. This first column then serves as a template for the subsequent deposition of TCO particles. These new particles tend to maximize the number of square−square contacts and thus minimize the total energy (Figure 7d−f and Movie S6). The nanowire packing as simulated in this way is shown in Figure 7g−i. As the simulation proceeds, additional TCOs become deposited; eventually, this results in conversion of the DHs formed initially into 3D superstructures analogous to what is observed in the crystalline state. These simulation studies thus provide support for the notion that the DH nanowires both are a substructure of the higher order TCO-based superstructure analyzed by X-ray diffraction analysis and can serve as a template for its growth. The premature lines of TCOs predicted to exist at the very initial stages of growth could be observed by STM by controlling the incubation time (Figure S25). The lines are seen at the bottom edge of the step (Figure S25b). Per our model, these incipient structures allow for the further growth of DH nanowires. Once a single nanowire is assembled, it perturbs the electronic structure of the nearby HOPG surface, leading to the formation of parallel nanowire pairs (for details see the SI). Moreover, with various incubation times (from 10 s to minutes), increasing numbers of parallel nanowires were observed by STM imaging from single chain to monolayer 2D arrays made up from numerous chains (Figure S22).

It is important to appreciate that, as with the 1D modeling, the self-assembled 3D superstructures obtained through simulations are more symmetric than those actually inferred from the studies of the HOPG-supported DHs. Nevertheless, there is a remarkably good match to experiment.

CONCLUSIONS

A giant spherical supramolecule with precisely controlled size and arrangement of porphyrin facets was successfully assembled through coordination-driven self-assembly. Such a complex supramolecule with the symmetry of a truncated cuboctahedron was observed to be packed on the HOPG surface into DH nanowires as a non-natural parastichy pattern. These nanowires were further transferred off the surface for fabricating an electronic device without losing integrity. A detailed simulation study revealed that the "sticky" interactions between ZP squares of two TCOs or the graphite surface guided the formation of the unprecedented packing behavior of the polyhedra.

This study leads us to propose that a combination of packing theory-based simulations and detailed studies of superstructures can advance our ability to synthesize large, rigid constructs from simple building blocks and understand how they will interact to produce self-assembled materials whose complexity matches that seen in the biological world. With the predictive capability of our model verified in the present instance, we suggest that a next step could involve the computational-based design of polyhedral supramolecular building blocks with optimized shapes, symmetries, and interactions to achieve new self-assembled structures. We also propose that it will prove possible to define the design space based on the area, distribution, and interaction range of the facet−facet contacts and employ either stochastic optimization or machine-learning-based methods to identify optimized features of the building blocks that will support the creation of highly complex structures. We are currently working along these lines.

ASSOCIATED CONTENT

Supporting Information

The Supporting Information is available free of charge at https://pubs.acs.org/doi/10.1021/jacs.1c00625.

Methods including synthetic details, TWIM-MS, AFM/SEM/TEM imaging, theoretical simulation, diffraction study, and $I-V$ test; more detailed data, including ^{1}H NMR, ^{13}C NMR, ^{31}P NMR, 2D COSY, 2D NOESY, ESI-MS, UV, and FL spectra of the complex; and additional AFM, TEM, and STM images (PDF)

Supporting movie (MP4)

Supporting movie (MP4)

Supporting movie (MP4)

Supporting movie (MP4)

Supporting movie (MP4)

Supporting movie (MP4)

Accession Codes

CCDC 2056916 contains the supplementary crystallographic data for this paper. These data can be obtained free of charge via www.ccdc.cam.ac.uk/data_request/cif, or by emailing data_request@ccdc.cam.ac.uk, or by contacting the Cambridge Crystallographic Data Centre, 12 Union Road, Cambridge CB2 1EZ, UK; fax: +44 1223 336033.

AUTHOR INFORMATION

Corresponding Authors

Jonathan L. Sessler − *Department of Chemistry, The University of Texas, Austin, Texas 78712, United States;* orcid.org/0000-0002-9576-1325; Email: sessler@cm.utexas.edu

Xiaopeng Li − *College of Chemistry and Environmental Engineering, Shenzhen University, Shenzhen, Guangdong 518060, China; Shenzhen University General Hospital, Shenzhen University Clinical Medical Academy, Shenzhen, Guangdong 518055, China;* orcid.org/0000-0001-9655-9551; Email: xiaopengli@szu.edu.cn

Authors

Heng Wang − *College of Chemistry and Environmental Engineering, Shenzhen University, Shenzhen, Guangdong 518060, China; Shenzhen University General Hospital, Shenzhen University Clinical Medical Academy, Shenzhen, Guangdong 518055, China*

Kun Wang − *Departments of Physics and Astronomy & Chemistry, Mississippi State University, Mississippi State, Mississippi 39762, United States*

Yaping Xu − *State Key Laboratory of Supramolecular Structure and Materials, College of Chemistry, Jilin University, Changchun, Jilin 130012, China*

Wu Wang − *Department of Physics, Southern University of Science and Technology, Shenzhen, Guangdong 518055, China*

Shaohua Chen − *School for Engineering of Matter, Transport and Energy, Arizona State University, Tempe, Arizona 85287, United States*

Matthew Hart − *School for Engineering of Matter, Transport and Energy, Arizona State University, Tempe, Arizona 85287, United States*

Lukasz Wojtas − *Department of Chemistry, University of South Florida, Tampa, Florida 33620, United States*

Li-Peng Zhou − *State Key Laboratory of Structural Chemistry, Fujian Institute of Research on the Structure of Matter, Chinese Academy of Sciences, Fuzhou 350002, China;* orcid.org/0000-0003-3820-2591

Lin Gan − *State Key Laboratory of Material Processing and Die & Mould Technology, School of Materials Science and Engineering, Huazhong University of Science and Technology, Wuhan, Hubei 430074, China*

Xuzhou Yan − *School of Chemistry and Chemical Engineering, Frontiers Science Center for Transformative Molecules, Shanghai Jiao Tong University, Shanghai 200240, China;* orcid.org/0000-0002-6114-5743

Yiming Li − *Department of Chemistry, University of South Florida, Tampa, Florida 33620, United States*

Juhoon Lee − *Department of Chemistry, The University of Texas, Austin, Texas 78712, United States*

Xian-Sheng Ke − *Department of Chemistry, The University of Texas, Austin, Texas 78712, United States*

Xu-Qing Wang − *Shanghai Key Laboratory of Green Chemistry and Chemical Processes, School of Chemistry and Molecular Engineering, East China Normal University, Shanghai 200062, China*

Chang-Wei Zhang − *Shanghai Key Laboratory of Green Chemistry and Chemical Processes, School of Chemistry and Molecular Engineering, East China Normal University, Shanghai 200062, China*

Shasha Zhou − *State Key Laboratory of Material Processing and Die & Mould Technology, School of Materials Science and Engineering, Huazhong University of Science and Technology, Wuhan, Hubei 430074, China*

Tianyou Zhai − *State Key Laboratory of Material Processing and Die & Mould Technology, School of Materials Science and Engineering, Huazhong University of Science and Technology, Wuhan, Hubei 430074, China;* orcid.org/0000-0003-0985-4806

Hai-Bo Yang − *Shanghai Key Laboratory of Green Chemistry and Chemical Processes, School of Chemistry and Molecular Engineering, East China Normal University, Shanghai 200062, China;* orcid.org/0000-0003-4926-1618

Ming Wang − *State Key Laboratory of Supramolecular Structure and Materials, College of Chemistry, Jilin University, Changchun, Jilin 130012, China;* orcid.org/0000-0002-5332-0804

Jiaqing He − *Department of Physics, Southern University of Science and Technology, Shenzhen, Guangdong 518055, China*

Qing-Fu Sun − *State Key Laboratory of Structural Chemistry, Fujian Institute of Research on the Structure of Matter, Chinese Academy of Sciences, Fuzhou 350002, China;* orcid.org/0000-0002-6419-8904

Bingqian Xu − *College of Engineering and Nanoscale Science and Engineering Center, University of Georgia, Athens, Georgia 30602, United States*

Yang Jiao − *School for Engineering of Matter, Transport and Energy, Arizona State University, Tempe, Arizona 85287, United States*

Peter J. Stang − *Department of Chemistry, University of Utah, Salt Lake City, Utah 84112, United States;* orcid.org/0000-0002-2307-0576

Complete contact information is available at: https://pubs.acs.org/10.1021/jacs.1c00625

Author Contributions

[#]H. Wang, K. Wang, Y. Xu, W. Wang contributed equally.

Notes

The authors declare no competing financial interest.

■ ACKNOWLEDGMENTS

X.L. acknowledges the Tencent Founders Alumni Foundation for support. This research was also supported in part by U.S. National Science Foundation (ECCS-1609788 to B.X.; CHE-1807152 to J.L.S.) and JLU Science and Technology Innovative Research Team (JLUSTIRT to M.W.). M.H. and Y.J. thank the FURI award from ASU. J.L.S. thanks the Robert A. Welch Foundation (F-0018) for partial support. The single-crystal diffraction data for compound TCO were collected at Argonne National Laboratory, Advanced Photon Source, Beamline 15-ID-B of ChemMatCARS. The beamline and PILATUS3 X CdTe 1M detector are principally supported by U.S. National Science Foundation (CHE-1346572 and DMR-1531283). Use of Advanced Photon Source, Office of Science User Facility operated for the U.S. Department of Energy (DOE) Office of Science by Argonne National Laboratory, is supported by the U.S. DOE (DE-AC02-06CH11357). We acknowledge the assistance of Mr. Chung-Hao Liu, Dr. Mu-Ping Nieh, and Dr. Lin Yang for their help with the SAXS analyses, as well as the support from the 16ID-LiX Beamline at the National Synchrotron Light Source II, Brookhaven National Laboratory (BNL), NY, USA. We thank Instrument Analysis Center and Electron Microscopy Center of Shenzhen University and the Pico Center of SUSTech Core Research Facilities for the TEM instrument usage. We also acknowledge the help from Dr. Yan Cao for discussion and analysis of HRTEM results.

■ REFERENCES

(1) Watson, J. D.; Crick, F. H. C. Molecular Structure of Nucleic Acids: A Structure for Deoxyribose Nucleic Acid. *Nature* **1953**, *171* (4356), 737−738.

(2) Erickson, R. O. Tubular Packing of Spheres in Biological Fine Structure. *Science* **1973**, *181* (4101), 705−716.

(3) Pennybacker, M. F.; Shipman, P. D.; Newell, A. C. Phyllotaxis: Some progress, but a story far from over. *Phys. D* **2015**, *306*, 48−81.

(4) Mitchison, G. J. Phyllotaxis and the Fibonacci Series. *Science* **1977**, *196* (4287), 270−275.
(5) Mughal, A.; Chan, H. K.; Weaire, D. Phyllotactic Description of Hard Sphere Packing in Cylindrical Channels. *Phys. Rev. Lett.* **2011**, *106* (11), 115704.
(6) Huxley, H. E. Electron microscope studies on the structure of natural and synthetic protein filaments from striated muscle. *J. Mol. Biol.* **1963**, *7* (3), 281−IN30.
(7) Adam, D.; Schuhmacher, P.; Simmerer, J.; Häussling, L.; Siemensmeyer, K.; Etzbachi, K. H.; Ringsdorf, H.; Haarer, D. Fast photoconduction in the highly ordered columnar phase of a discotic liquid crystal. *Nature* **1994**, *371* (6493), 141−143.
(8) Percec, V.; Glodde, M.; Bera, T. K.; Miura, Y.; Shiyanovskaya, I.; Singer, K. D.; Balagurusamy, V. S. K.; Heiney, P. A.; Schnell, I.; Rapp, A.; Spiess, H. W.; Hudson, S. D.; Duan, H. Self-organization of supramolecular helical dendrimers into complex electronic materials. *Nature* **2002**, *419* (6905), 384−387.
(9) Kanibolotsky, A. L.; Perepichka, I. F.; Skabara, P. J. Star-shaped π-conjugated oligomers and their applications in organic electronics and photonics. *Chem. Soc. Rev.* **2010**, *39* (7), 2695−2728.
(10) Li, F.; Josephson, D. P.; Stein, A. Colloidal Assembly: The Road from Particles to Colloidal Molecules and Crystals. *Angew. Chem., Int. Ed.* **2011**, *50* (2), 360−388.
(11) Glotzer, S. C.; Solomon, M. J. Anisotropy of building blocks and their assembly into complex structures. *Nat. Mater.* **2007**, *6* (8), 557−562.
(12) Cook, T. R.; Stang, P. J. Recent Developments in the Preparation and Chemistry of Metallacycles and Metallacages via Coordination. *Chem. Rev.* **2015**, *115* (15), 7001−7045.
(13) Olenyuk, B.; Whiteford, J. A.; Fechtenkötter, A.; Stang, P. J. Self-assembly of nanoscale cuboctahedra by coordination chemistry. *Nature* **1999**, *398* (6730), 796−799.
(14) Chichak, K. S.; Cantrill, S. J.; Pease, A. R.; Chiu, S.-H.; Cave, G. W. V.; Atwood, J. L.; Stoddart, J. F. Molecular Borromean Rings. *Science* **2004**, *304* (5675), 1308−1312.
(15) McKinlay, R. M.; Cave, G. W. V.; Atwood, J. L. Supramolecular blueprint approach to metal-coordinated capsules. *Proc. Natl. Acad. Sci. U. S. A.* **2005**, *102* (17), 5944−5948.
(16) Newkome, G. R.; Wang, P.; Moorefield, C. N.; Cho, T. J.; Mohapatra, P. P.; Li, S.; Hwang, S.-H.; Lukoyanova, O.; Echegoyen, L.; Palagallo, J. A.; Iancu, V.; Hla, S.-W. Nanoassembly of a Fractal Polymer: A Molecular "Sierpinski Hexagonal Gasket. *Science* **2006**, *312* (5781), 1782−1785.
(17) Hiraoka, S.; Harano, K.; Shiro, M.; Ozawa, Y.; Yasuda, N.; Toriumi, K.; Shionoya, M. Isostructural Coordination Capsules for a Series of 10 Different d_5−d_{10} Transition-Metal Ions. *Angew. Chem., Int. Ed.* **2006**, *45* (39), 6488−6491.
(18) Pluth, M. D.; Bergman, R. G.; Raymond, K. N. Acid Catalysis in Basic Solution: A Supramolecular Host Promotes Orthoformate Hydrolysis. *Science* **2007**, *316* (5821), 85−88.
(19) Bar, A. K.; Chakrabarty, R.; Mostafa, G.; Mukherjee, P. S. Self-Assembly of a Nanoscopic $Pt_{12}Fe_{12}$ Heterometallic Open Molecular Box Containing Six Porphyrin Walls. *Angew. Chem., Int. Ed.* **2008**, *47* (44), 8455−8459.
(20) Sun, Q.-F.; Iwasa, J.; Ogawa, D.; Ishido, Y.; Sato, S.; Ozeki, T.; Sei, Y.; Yamaguchi, K.; Fujita, M. Self-Assembled $M_{24}L_{48}$ Polyhedra and Their Sharp Structural Switch upon Subtle Ligand Variation. *Science* **2010**, *328* (5982), 1144−1147.
(21) Fujita, D.; Ueda, Y.; Sato, S.; Mizuno, N.; Kumasaka, T.; Fujita, M. Self-assembly of tetravalent Goldberg polyhedra from 144 small components. *Nature* **2016**, *540* (7634), 563−566.
(22) Fujita, D.; Ueda, Y.; Sato, S.; Yokoyama, H.; Mizuno, N.; Kumasaka, T.; Fujita, M. Self-Assembly of $M_{30}L_{60}$ Icosidodecahedron. *Chem.* **2016**, *1* (1), 91−101.
(23) Marcos, V.; Stephens, A. J.; Jaramillo-Garcia, J.; Nussbaumer, A. L.; Woltering, S. L.; Valero, A.; Lemonnier, J.-F.; Vitorica-Yrezabal, I. J.; Leigh, D. A. Allosteric initiation and regulation of catalysis with a molecular knot. *Science* **2016**, *352* (6293), 1555−1559.
(24) Zhiquan, L.; Polen, S.; Hadad, C. M.; RajanBabu, T. V.; Badjić, J. D. Russian Nesting Doll Complexes of Molecular Baskets and Zinc Containing TPA Ligands. *J. Am. Chem. Soc.* **2016**, *138* (26), 8253−8258.
(25) Rizzuto, F. J.; Nitschke, J. R. Stereochemical plasticity modulates cooperative binding in a $Co^{II}_{12}L_6$ cuboctahedron. *Nat. Chem.* **2017**, *9* (9), 903−908.
(26) Samanta, S. K.; Quigley, J.; Vinciguerra, B.; Briken, V.; Isaacs, L. Cucurbit[7]uril Enables Multi-Stimuli-Responsive Release from the Self-Assembled Hydrophobic Phase of a Metal Organic Polyhedron. *J. Am. Chem. Soc.* **2017**, *139* (26), 9066−9074.
(27) Gu, Y.; Alt, E. A.; Wang, H.; Li, X.; Willard, A. P.; Johnson, J. A. Photoswitching topology in polymer networks with metal−organic cages as crosslinks. *Nature* **2018**, *560* (7716), 65−69.
(28) Hou, Y.-J.; Wu, K.; Wei, Z.-W.; Li, K.; Lu, Y.-L.; Zhu, C.-Y.; Wang, J.-S.; Pan, M.; Jiang, J.-J.; Li, G.-Q.; Su, C.-Y. Design and Enantioresolution of Homochiral Fe(II)−Pd(II) Coordination Cages from Stereolabile Metalloligands: Stereochemical Stability and Enantioselective Separation. *J. Am. Chem. Soc.* **2018**, *140* (51), 18183−18191.
(29) Wang, H.; Zhou, L.-P.; Zheng, Y.; Wang, K.; Song, B.; Yan, X.; Wojtas, L.; Wang, X.-Q.; Jiang, X.; Wang, M.; Sun, Q.-F.; Xu, B.; Yang, H.-B.; Sue, A. C.-H.; Chan, Y.-T.; Sessler, J. L.; Jiao, Y.; Stang, P. J.; Li, X. Double-Layered Supramolecular Prisms Self-Assembled by Geometrically Non-equivalent Tetratopic Subunits. *Angew. Chem., Int. Ed.* **2021**, *60* (3), 1298−1305.
(30) Boerdijk, A. Some remarks concerning close-packing of equal spheres. *Philips Res. Rep.* **1952**, *7*, 303−313.
(31) Coxeter, H. S. M. The Simplicial Helix and the Equation tan $n\theta$ = n tan θ. *Can. Math. Bull.* **1985**, *28* (4), 385−393.
(32) Haji-Akbari, A.; Engel, M.; Keys, A. S.; Zheng, X.; Petschek, R. G.; Palffy-Muhoray, P.; Glotzer, S. C. Disordered, quasicrystalline and crystalline phases of densely packed tetrahedra. *Nature* **2009**, *462* (7274), 773−777.
(33) Koo, J.; Kim, I.; Kim, Y.; Cho, D.; Hwang, I.-C.; Mukhopadhyay, R. D.; Song, H.; Ko, Y. H.; Dhamija, A.; Lee, H.; Hwang, W.; Kim, S.; Baik, M.-H.; Kim, K. Gigantic Porphyrinic Cages. *Chem.* **2020**, *6* (12), 3374−3384.
(34) Wlodawer, A.; Minor, W.; Dauter, Z.; Jaskolski, M. Protein crystallography for non-crystallographers, or how to get the best (but not more) from published macromolecular structures. *FEBS J.* **2008**, *275* (1), 1−21.
(35) Allen, J. P.; Feher, G.; Yeates, T. O.; Komiya, H.; Rees, D. C. Structure of the reaction center from Rhodobacter sphaeroides R-26: the protein subunits. *Proc. Natl. Acad. Sci. U. S. A.* **1987**, *84* (17), 6162−6166.
(36) Yokoyama, T.; Yokoyama, S.; Kamikado, T.; Okuno, Y.; Mashiko, S. Selective assembly on a surface of supramolecular aggregates with controlled size and shape. *Nature* **2001**, *413*, 619.
(37) Grill, L.; Dyer, M.; Lafferentz, L.; Persson, M.; Peters, M. V.; Hecht, S. Nano-architectures by covalent assembly of molecular building blocks. *Nat. Nanotechnol.* **2007**, *2*, 687.
(38) Wintjes, N.; Bonifazi, D.; Cheng, F.; Kiebele, A.; Stöhr, M.; Jung, T.; Spillmann, H.; Diederich, F. A Supramolecular Multiposition Rotary Device. *Angew. Chem., Int. Ed.* **2007**, *46* (22), 4089−4092.
(39) O'Sullivan, M. C.; Sprafke, J. K.; Kondratuk, D. V.; Rinfray, C.; Claridge, T. D. W.; Saywell, A.; Blunt, M. O.; O'Shea, J. N.; Beton, P. H.; Malfois, M.; Anderson, H. L. Vernier templating and synthesis of a 12-porphyrin nano-ring. *Nature* **2011**, *469*, 72.
(40) Katsonis, N.; Vicario, J.; Kudernac, T.; Visser, J.; Pollard, M. M.; Feringa, B. L. Self-Organized Monolayer of meso-Tetradodecylporphyrin Coordinated to Au(111). *J. Am. Chem. Soc.* **2006**, *128* (48), 15537−15541.
(41) den Boer, D.; Li, M.; Habets, T.; Iavicoli, P.; Rowan, A. E.; Nolte, R. J. M.; Speller, S.; Amabilino, D. B.; De Feyter, S.; Elemans, J. A. A. W. Detection of different oxidation states of individual manganese porphyrins during their reaction with oxygen at a solid/liquid interface. *Nat. Chem.* **2013**, *5*, 621.

https://doi.org/10.1021/jacs.1c00625
J. Am. Chem. Soc. 2021, 143, 5826−5835

(42) Peng, X.; Komatsu, N.; Bhattacharya, S.; Shimawaki, T.; Aonuma, S.; Kimura, T.; Osuka, A. Optically active single-walled carbon nanotubes. *Nat. Nanotechnol.* **2007**, *2*, 361.
(43) Zach, M. P.; Ng, K. H.; Penner, R. M. Molybdenum Nanowires by Electrodeposition. *Science* **2000**, *290* (5499), 2120−2123.
(44) Simonis, P.; Goffaux, C.; Thiry, P. A.; Biro, L. P.; Lambin, P.; Meunier, V. STM study of a grain boundary in graphite. *Surf. Sci.* **2002**, *511* (1), 319−322.
(45) Smoluchowski, R. Anisotropy of the Electronic Work Function of Metals. *Phys. Rev.* **1941**, *60* (9), 661−674.
(46) Stranick, S. J.; Kamna, M. M.; Weiss, P. S. Atomic-Scale Dynamics of a Two-Dimensional Gas-Solid Interface. *Science* **1994**, *266* (5182), 99−102.
(47) Kamna, M. M.; Stranick, S. J.; Weiss, P. S. Imaging Substrate-Mediated Interactions. *Science* **1996**, *274* (5284), 118−119.
(48) Torquato, S.; Jiao, Y. Dense packings of the Platonic and Archimedean solids. *Nature* **2009**, *460* (7257), 876−879.
(49) Agarwal, U.; Escobedo, F. A. Mesophase behaviour of polyhedral particles. *Nat. Mater.* **2011**, *10*, 230.
(50) Damasceno, P. F.; Engel, M.; Glotzer, S. C. Predictive self-assembly of polyhedra into complex structures. *Science* **2012**, *337* (6093), 453−457.
(51) de Graaf, J.; van Roij, R.; Dijkstra, M. Dense regular packings of irregular nonconvex particles. *Phys. Rev. Lett.* **2011**, *107* (15), 155501.
(52) Avci, C.; Imaz, I.; Carné-Sánchez, A.; Pariente, J. A.; Tasios, N.; Pérez-Carvajal, J.; Alonso, M. I.; Blanco, A.; Dijkstra, M.; López, C.; Maspoch, D. Self-assembly of polyhedral metal−organic framework particles into three-dimensional ordered superstructures. *Nat. Chem.* **2018**, *10*, 78.
(53) Ye, X.; Chen, J.; Engel, M.; Millan, J. A.; Li, W.; Qi, L.; Xing, G.; Collins, J. E.; Kagan, C. R.; Li, J.; Glotzer, S. C.; Murray, C. B. Competition of shape and interaction patchiness for self-assembling nanoplates. *Nat. Chem.* **2013**, *5*, 466.
(54) Henzie, J.; Grünwald, M.; Widmer-Cooper, A.; Geissler, P. L.; Yang, P. Self-assembly of uniform polyhedral silver nanocrystals into densest packings and exotic superlattices. *Nat. Mater.* **2012**, *11*, 131.
(55) de Nijs, B.; Dussi, S.; Smallenburg, F.; Meeldijk, J. D.; roenendijk, D. J.; Filion, L.; Imhof, A.; van Blaaderen, A.; Dijkstra, M. Entropy-driven formation of large icosahedral colloidal clusters by spherical confinement. *Nat. Mater.* **2015**, *14*, 56.
(56) Singh, G.; Chan, H.; Baskin, A.; Gelman, E.; Repnin, N.; Král, P.; Klajn, R. Self-assembly of magnetite nanocubes into helical superstructures. *Science* **2014**, *345* (6201), 1149−1153.
(57) Lin, H.; Lee, S.; Sun, L.; Spellings, M.; Engel, M.; Glotzer, S. C.; Mirkin, C. A. Clathrate colloidal crystals. *Science* **2017**, *355* (6328), 931−935.
(58) Teich, E. G.; van Anders, G.; Klotsa, D.; Dshemuchadse, J.; Glotzer, S. C. Clusters of polyhedra in spherical confinement. *Proc. Natl. Acad. Sci. U. S. A.* **2016**, *113* (6), E669−E678.

https://doi.org/10.1021/jacs.1c00625
J. Am. Chem. Soc. 2021, 143, 5826−5835